Aerospace Science and Technology 38 (2014) 30–40

Contents lists available at ScienceDirect

Aerospace Science and Technology

www.elsevier.com/locate/aescte

A reaction-null/Jacobian transpose control strategy with gravity gradient compensation for on-orbit space manipulators

A. Pisculli [a,*], L. Felicetti [b], P. Gasbarri [a], G.B. Palmerini [b], M. Sabatini [b]

[a] DIMA – Dipartimento di Ingegneria Meccanica ed Aerospaziale, University of Rome "La Sapienza", via Eudossiana 18, 00184 Roma, Italy
[b] DIAEE – Dipartimento di Ingegneria Astronautica Elettrica ed Energetica, University of Rome "La Sapienza", via Salaria 851, 00138 Roma, Italy

ARTICLE INFO

Article history:
Received 9 April 2014
Received in revised form 10 June 2014
Accepted 27 July 2014
Available online 4 August 2014

Keywords:
Space manipulator
Reaction null control
Jacobian transpose control
Gravity gradient compensation
Space multibody dynamics

ABSTRACT

The dynamics and the control of space manipulators floating in 3D space is analyzed in this paper. A minimum state variable approach for describing the dynamics of a free-floating space manipulator under gravity and gravity gradient forces is presented. A new control strategy involving a combination of Reaction Null and Jacobian Transpose controllers, including also the gravity gradient compensation, is suggested and compared with the Jacobian Transpose control and the conventional Proportional Derivative control. Several numerical examples will be presented and discussed, considering platforms with single and double manipulators, showing the advantages and drawbacks related to these control strategies.

1. Introduction

Recent proposals for missions involving the use of space manipulators are presented as a solution for several problems which now affect the operations and the performance of in-orbit space systems. In the past several rendez-vous and docking missions have been performed by means of robotic manipulators [28]; the same manipulators have been used to handle and assemble large space modules and to reduce human extravehicular activities [2,14,20]. Many studies have been also performed to verify the possibility to extend the operational life of the commercial and scientific satellites through an automatic servicing spacecraft dedicated to repair, refuel and/or manage their failures [21]. Furthermore, active debris removal via robotic systems is one of the main concerns that governments and space agencies are facing in the last years [4,17–19].

Of course one of the main tasks for a space manipulator is to deploy its robotic arms to reach a target. Indeed, since the robotic arms are attached to a floating/orbiting platform, their motion produces an unwanted motion of the platform, too. In particular the attitude of the platform could be modified in such a way that the manipulator could not be able to deploy its arms in a correct way to reach the target. Classic deploying algorithms and techniques used for fixed base manipulators [27] cannot be used in space and special attitude control strategies, which take the floating base condition into account, should be implemented. These control strategies have to consider also the maximum allowable torque supplied by the attitude actuators, the power consumption, and the computational capabilities of the on-board computing devices. Among all the possible strategies to move robotic arms, the so-called Reaction Null Control Strategy (RNCS) guarantees the required tasks with a null disturbance on the attitude of the base spacecraft platform as reported in Refs. [7,35]. The same studies have shown that one of the main limitations of the RNCS, applied to a 2D floating robotic system, is that not all the points of its geometric workspace can be reached by the end-effector of the manipulator. An extension to a 3D case, although analytically addressed in Refs. [6,26], was not verified numerically. Furthermore, different control strategies other the one of RNCS have been proposed in the past for controlling the motion of a robotic space manipulator to capture an orbiting satellite including an attitude control of the base platform [30,32], but not compared with RNCS control in terms of performances and/or applicability.

In this work a comparison of different control algorithms, applied to a full 3D floating and gravity gradient perturbed robotic system, is presented and discussed. In particular the Jacobian Transpose Control strategy (JTC) and the classic Proportional Derivative Control Strategy are compared with the RNCS in terms of performance, power consumption and effectiveness for deploying the arms and grasping a target. This comparison will be useful to evaluate the benefits and the drawbacks of the three control schemes and for a better understanding of their applicability in a fully tridimensional space environment. Later on a new control strategy involving a combination of the RNCS and the JTC, including also the gravity gradient compensation, is suggested as

* Corresponding author.

http://dx.doi.org/10.1016/j.ast.2014.07.012
1270-9638/

a solution for space manipulator deploying and maneuvering. Even though both the RNCS and the JTC must be considered well-known control techniques, their combined application to the case of a full 3D floating dynamic system has not be deeply investigated yet at the best of the authors knowledge, and this is one of the major contributions of this work. The paper is organized as follows: in Section 2 the derivation of the equation of motion for floating deployable structures is exposed. In particular, starting from the kinematical analysis of the system, the relationship which characterizes the joints is derived and included into a Jacobian matrix. This Jacobian matrix will also be used for describing the dynamics of the system, and in particular it will be employed for reducing the entire set of the equations of motion to a minimum set with a minimum variables formulation. The gravitational and the gravity gradient effects are also included into the formulation, in order to proficiently simulate the space environment conditions applied to the multibody system. The resulting set of equations of motion permits the simulation and the analysis of the problems highlighted before. In Section 3 the proportional derivative control, the Jacobian transpose based control and the Reaction Null control are described. In Section 4 numerical results of a space manipulator system exploiting the deploying maneuvers are presented. Different cases of the deploying maneuvers are then analyzed, in order to evaluate the proficiency and the efforts necessary for applying different suggested control schemes to the system. The paper will be closed with a discussion of the results and the relevant concluding remarks in Section 5.

2. Mathematical model for floating multibody systems

The deployment of space structures has been widely analyzed by using multibody formulations [11,25,31,33]. Generally the two leading approaches are Newton–Euler (NE) and Euler–Lagrange (EL) approach [24]. Both of them present advantages and drawbacks. Indeed the NE approach considers a complete set of equations of motion for each single body belonging to the system, with their coordinates not dependent on the multibody topology. Moreover it applies the constraints' equations in order to represent the kinematic connection between two adjacent bodies, leading to a Differential Algebraic Equations (DAE) of motion. On the other hand the EL approach derives the equations of motion starting from the kinetic, elastic and gravitational functionals for the applications of the Hamilton's principle [9,24]. Of course, following this methodology, we can obtain a minimum set of Ordinary Differential Equation (ODE) which describes the behavior of the multibody system dynamics. The main advantage is that no constraint equations must be included as for the NE approach. On the contrary the NE formulation enables a simpler assembling of the dynamic equations of complex multibody configurations that can be easily implemented in a numerical code. In addition the NE approach directly provides the reaction forces among the bodies [22,29]. This is more complicated to obtain from the EL formulation.

The ideal formulation for describing multibody systems should be represented by a combination between the two methodologies. It can be obtained by analyzing the NE formulation for assembling the equation of motion into account and then by describing the ODE governing equations by a minimum set of variables as suggested by Kane in [12,13]. This method allows to easily analyze multibody systems with pre-determined constraints. In this paper a Kane-like formulation is adopted to obtain a system of equations of motion which can also be suitable for synthesizing optimal control strategies during the deploying maneuvers. The proposed method differs from the classic one for two different aspects: (i) the reference frame, which all the *other* bodies motions are referred to, is a floating reference frame attached to the base platform body; (ii) it leads to a more organic formulation and

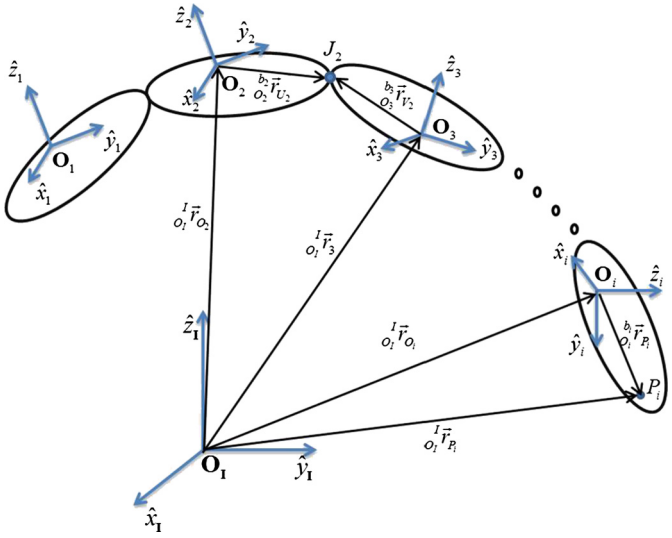

Fig. 1. Reference frames associated to the multibody system.

to a transformation between the NE and the EL (and vice versa) through the use of a Jacobian matrix as it will be shown in Section 2.3.

2.1. Kinematics of a tridimensional floating multibody platform

Let us assume that the space multibody system can be represented by N rigid bodies interconnected by $N-1$ joints, leading to a serial kinematic chain, as shown in Fig. 1. Let us associate a reference frame to each body b_i of the kinematic chain. The position of the origin (O_i) of this reference frame with respect to the origin of the inertial reference frame (O_I) can be indicated by the vector ${}^{I}_{O_I}\vec{r}_{O_i}$, where the bottom right index represents the end-point of the vector $\vec{r}$ and the bottom and upper left indexes represent the origin (O_I) and the reference frame (I) which the same vector is referred to, respectively. In a similar way, the attitude of the body b_i is represented by a transformation matrix ${}^{I}\mathbf{T}_{b_i}$, which rotates the coordinates from the reference frame detected by the bottom right index (b_i) to the reference frame represented by the upper left index (I).

The position vector of a generic point P_i belonging to the i-th body can be represented by the following relation [23]:

$$ {}^{I}_{O_I}\vec{r}_{P_i} = {}^{I}_{O_I}\vec{r}_{O_i} + {}^{I}\mathbf{T}_{b_i}\, {}^{b_i}_{O_I}\vec{r}_{P_i} \tag{1} $$

The position of the point P_i can be also expressed with respect to the previous body reference frame (the $(i-1)$-th) as follows:

$$ \begin{aligned} {}^{I}_{O_I}\vec{r}_{P_i} = {}^{I}_{O_I}\vec{r}_{O_{i-1}} + {}^{I}\mathbf{T}_{b_{i-1}}\, {}^{b_{i-1}}_{O_{i-1}}\vec{r}_{U_{i-1}} + {}^{I}\mathbf{T}_{b_{i-1}}\, {}^{b_{i-1}}_{U_{i-1}}\vec{j}_{i-1} \\ - {}^{I}\mathbf{T}_{b_i}\, {}^{b_i}_{O_i}\vec{r}_{V_{i-1}} + {}^{I}\mathbf{T}_{b_i}\, {}^{b_i}_{O_i}\vec{r}_{P_i} \end{aligned} \tag{2} $$

Eq. (2) can be easily determined by a geometrical consideration, as shown in Fig. 1.

The joint vector (JV) ${}^{b_{i-1}}_{J_{i-1}}\vec{j}_{i-1}$ represents the relative position between the joint node V_{i-1} of the i-th body and the joint node U_{i-1} of the $(i-1)$-th body, connected through the $(i-1)$-th joint, as highlighted in Fig. 2. The JV is strictly dependent on the joint typology. For instance the JV is a null vector in the spherical or revolute joints, leading to the following constraint:

$$ {}^{b_{i-1}}_{U_{i-1}}\vec{j}_{i-1} = 0 \tag{3} $$

whereas, in the prismatic joint case, it can be represented by:

$$ {}^{b_{i-1}}_{U_{i-1}}\vec{j}_{i-1} = {}^{b_{i-1}}_{U_{i-1}}\hat{u}_{i-1} q_{i-1} \tag{4} $$

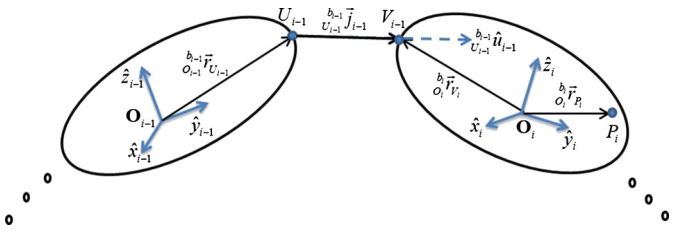

Fig. 2. Joint vector definition.

where the unit vector ${}^{b_{i-1}}_{U_{i-1}}\hat{u}_{i-1}$ is the direction of the relative translation between the i-th and $(i-1)$-th bodies and q_{i-1} is the joint variable.

The velocity of the point mass P_i of the i-th body can be easily obtained by deriving Eq. (2) with respect to time:

$$\begin{aligned}{}^{I}_{O_I}\dot{\vec{r}}_{P_i} &= {}^{I}_{O_I}\dot{\vec{r}}_{O_{i-1}} + {}^{I}_{I}\Omega_{b_{i-1}}\,{}^{I}\mathbf{T}_{b_{i-1}}\,{}^{b_{i-1}}_{O_{i-1}}\vec{r}_{U_{i-1}} \\ &\quad + {}^{I}_{I}\Omega_{b_{i-1}}\,{}^{I}\mathbf{T}_{b_{i-1}}\,{}^{b_{i-1}}_{U_{i-1}}\hat{u}_{i-1}q_{i-1} + {}^{I}\mathbf{T}_{b_{i-1}}\,{}^{b_{i-1}}_{U_{i-1}}\hat{u}_{i-1}\dot{q}_{i-1} \\ &\quad - {}^{I}_{I}\Omega_{b_i}\,{}^{I}\mathbf{T}_{b_i}\,{}^{b_i}_{O_i}\vec{r}_{V_{i-1}} + {}^{I}_{I}\Omega_{b_i}\,{}^{I}\mathbf{T}_{b_i}\,{}^{b_i}_{O_i}\vec{r}_{P_i}\end{aligned} \tag{5}$$

where the upper dot represents the time derivative in the inertial frame and ${}^{I}_{I}\Omega_{b_i}$ is the skew-symmetric matrix associated to the angular velocity of the i-th body, around the inertial reference frame and whose components (ω_1, ω_2 and ω_3) are referred to the inertial reference frame. The skew-symmetric matrix ${}^{I}_{I}\Omega_{b_i}$ is obtained by:

$${}^{I}_{I}\Omega_{b_i} = {}^{I}\dot{\mathbf{T}}_{b_i}\,{}^{I}\mathbf{T}^{T}_{b_i} = \begin{bmatrix} 0 & -\omega_3 & \omega_2 \\ \omega_3 & 0 & -\omega_1 \\ -\omega_2 & \omega_1 & 0 \end{bmatrix} \tag{6}$$

Note that the relative angular velocity between two bodies can be represented by the following relation:

$$\begin{aligned}{}^{b_{i-1}}_{I}\Omega_{b_i} &= {}^{I}_{I}\Omega_{b_i} - {}^{I}_{I}\Omega_{b_{i-1}} \\ &= {}^{I}\mathbf{T}_{b_i}\left({}^{b_i}_{I}\Omega_{b_i} - {}^{b_i}\mathbf{T}_{b_{i-1}}\,{}^{b_{i-1}}_{I}\Omega_{b_{i-1}}\right){}^{I}\mathbf{T}^{T}_{b_i} \\ &= {}^{I}\mathbf{T}_{b_i}\,{}^{b_i}_{b_{i-1}}\Omega_{b_i}\,{}^{I}\mathbf{T}^{T}_{b_i}\end{aligned} \tag{7}$$

where the matrix ${}^{b_i}_{b_{i-1}}\Omega_{b_i}$ can take different forms depending on the type of joints adopted to connect two adjacent bodies. In the spherical joints all rotations are allowed, whereas a revolute joint permits only one direction of rotation leading to:

$${}^{b_i}_{b_{i-1}}\Omega_{b_i} = \begin{bmatrix} 0 & -z_3 & z_2 \\ z_3 & 0 & -z_1 \\ -z_2 & z_1 & 0 \end{bmatrix}\dot{\theta}_{i-1} \tag{8}$$

In the above matrix the unit vector $\hat{z}_i = (z_1 \quad z_2 \quad z_3)^T_i$ represents the rotation axis of the $(i-1)$-th revolute joint, that is fixed in the i-th body reference frame. Finally, for the prismatic joint case, we have the condition ${}^{b_i}_{b_{i-1}}\Omega_{b_i} = 0$.

Through the time derivative of Eq. (5) it is of course possible to obtain the acceleration of the point P_i with respect to the $(i-1)$-th reference frame:

$$\begin{aligned}\frac{d^I}{dt}\,{}^{I}_{O_I}\dot{\vec{r}}_{P_i} &= {}^{I}_{O_I}\ddot{\vec{r}}_{O_{i-1}} + {}^{I}_{I}\Omega_{b_{i-1}}\,{}^{I}_{I}\Omega_{b_{i-1}}\,{}^{I}\mathbf{T}_{b_{i-1}}\,{}^{b_{i-1}}_{O_{i-1}}\vec{r}_{U_{i-1}} \\ &\quad + {}^{I}_{I}\dot{\Omega}_{b_{i-1}}\,{}^{I}\mathbf{T}_{b_{i-1}}\,{}^{b_{i-1}}_{O_{i-1}}\vec{r}_{U_{i-1}} - {}^{I}_{I}\Omega_{b_i}\,{}^{I}_{I}\Omega_{b_i}\,{}^{I}\mathbf{T}_{b_i}\,{}^{b_i}_{O_i}\vec{r}_{V_{i-1}} \\ &\quad - {}^{I}_{I}\dot{\Omega}_{b_i}\,{}^{I}\mathbf{T}_{b_i}\,{}^{b_i}_{O_i}\vec{r}_{V_{i-1}} + {}^{I}_{I}\Omega_{b_i}\,{}^{I}_{I}\Omega_{b_i}\,{}^{I}\mathbf{T}_{b_i}\,{}^{b_i}_{O_i}\vec{r}_{P_i} \\ &\quad + {}^{I}_{I}\dot{\Omega}_{b_i}\,{}^{I}\mathbf{T}_{b_i}\,{}^{b_i}_{O_i}\vec{r}_{P_i} + {}^{I}_{I}\Omega_{b_{i-1}}\,{}^{I}_{I}\Omega_{b_{i-1}}\,{}^{I}\mathbf{T}_{b_{i-1}}\,{}^{b_{i-1}}_{U_{i-1}}\hat{u}_{i-1}q_{i-1} \\ &\quad + {}^{I}_{I}\dot{\Omega}_{b_{i-1}}\,{}^{I}\mathbf{T}_{b_{i-1}}\,{}^{b_{i-1}}_{U_{i-1}}\hat{u}_{i-1}q_{i-1} \\ &\quad + 2\,{}^{I}_{I}\Omega_{b_{i-1}}\,{}^{I}\mathbf{T}_{b_{i-1}}\,{}^{b_{i-1}}_{U_{i-1}}\hat{u}_{i-1}\dot{q}_{i-1} + {}^{I}\mathbf{T}_{b_{i-1}}\,{}^{b_{i-1}}_{U_{i-1}}\hat{u}_{i-1}\ddot{q}_{i-1}\end{aligned} \tag{9}$$

The recursive application of Eq. (5) leads to the determination of the Jacobian matrix $\mathbf{J}$ which allows to calculate the Cartesian velocities as a function of the multibody joint velocities:

$$\dot{X} = \mathbf{J}\dot{Q} \tag{10}$$

where the state space vector, including the Cartesian velocities, is:

$$\dot{X} = \left[\,{}^{I}_{O_I}\dot{\vec{r}}_{O_1}{}^T \quad {}^{I}_{I}\vec{\omega}_{b_1}{}^T \quad {}^{I}_{O_I}\dot{\vec{r}}_{O_2}{}^T \quad {}^{I}_{I}\vec{\omega}_{b_2}{}^T \quad \cdots \quad {}^{I}_{O_I}\dot{\vec{r}}_{O_N}{}^T \quad {}^{I}_{I}\vec{\omega}_{b_N}{}^T\,\right]^T \tag{11}$$

and the joint velocities state space vector is:

$$\begin{aligned}\dot{Q} = \big[\,{}^{I}_{O_I}\dot{\vec{r}}_{O_1}{}^T \quad {}^{I}_{I}\vec{\omega}_{b_1}{}^T \quad \dot{\theta}_1 \quad \cdots \quad \dot{\theta}_r\dot{q}_{r+1} \quad \cdots \quad \dot{q}_{r+p} \quad \vec{\omega}_{r+p+1}{}^T \\ \cdots \quad \vec{\omega}_{r+p+s}{}^T\,\big]^T\end{aligned} \tag{12}$$

which is constituted by the linear (${}^{I}_{O_I}\dot{\vec{r}}_{O_1}$) and angular (${}^{I}_{I}\vec{\omega}_{b_1}$) velocities of the first body, the r revolute angular velocities ($\dot{\theta}_1$), the p prismatic velocities ($\dot{q}_{r+1}$) and the s spherical angular velocities ($\vec{\omega}_{r+p+1}$).

2.2. Fully equation of a dynamic multibody system

The translational and rotational equilibrium equations of each single body of the multibody system can be written as follows:

$$m_i\frac{d}{dt}\left[{}^{I}_{O_I}\dot{\vec{r}}_{O_i} + {}^{I}_{I}\Omega_{b_i}\,{}^{I}_{O_i}\vec{r}_{cm_i}\right] = {}^{I}\vec{F}^{ext}_{b_i} \tag{13}$$

$$\frac{d}{dt}\left[{}^{I}_{O_i}\mathbf{I}_{b_i}\,{}^{I}_{I}\vec{\omega}_{b_i} + m_i\,{}^{I}_{O_i}\tilde{r}_{cm_i}\,{}^{I}_{O_I}\dot{\vec{r}}_{b_i}\right] = {}^{I}_{O_i}\vec{M}^{ext}_{b_i} + m_i\,{}^{I}_{I}\Omega_{b_i}\,{}^{I}_{O_i}\tilde{r}_{cm_i}\,{}^{I}_{O_I}\dot{\vec{r}}_{b_i} \tag{14}$$

where m_i is the mass and ${}^{I}_{O_i}\mathbf{I}_{b_i}$ the inertia matrix of the i-th body whereas the vector ${}^{I}_{O_i}\vec{r}_{cm_i}$ is the distance of the center of mass of the body with respect to the origin of the body reference frame; ${}^{I}\vec{F}^{ext}_{b_i}$ and ${}^{I}_{O_i}\vec{M}^{ext}_{b_i}$ are the external forces and torques applied to the i-th body respectively. The symbol ($\sim$) in Eq. (14) represents the skew symmetric form of the relevant vector. Eq. (13) and Eq. (14) are the general equations of rigid bodies; note that no hypotheses are made on the kinematics of possible interconnected bodies.

These joints reduce the relative motion of the links which represent the arms of the manipulator. In order to describe this constrained kinematics it is necessary to introduce appropriate compatibility equations between the bodies. Holonomic and sclero-nomic constraint equations can be represented in an algebraic form [1,15] as follows:

$$\Psi(X,t) = 0 \tag{15}$$

As previously stated, Eq. (13) and Eq. (14), complemented with the generalized unknown reaction forces, must respect the constraints described by Eq. (15). This leads to the resolution of a Differential Algebraic Equations (DAE) system. A possible approach to solve this problem is to transform the DAE into a fully Ordinary Differential Equation (ODE) system by double deriving Eq. (15) with respect to time [8]:

$$\begin{aligned}&\Psi_{,X}\dot{X} = 0 \\ &\Psi_{,X}\ddot{X} + \dot{\Psi}_{,X}\dot{X} = 0\end{aligned} \tag{16}$$

In Eq. (16) the matrix $\Psi_{,X}$ represents the Jacobian matrix, which contains the partial derivatives of Eq. (15) with respect to the state space vector. The generalized reaction forces and torques are defined as $R = -\Psi^T_{,X}\Lambda$ (where Λ is the unknown vector of the Lagrangian multipliers). Of course R must guarantee the kinematic compatibility between two connected bodies and can be evaluated by combining Eq. (13) and Eq. (14) with Eq. (16). The resulting

matrix form of this combination represents the so-called NE formulation of the equation of motion for a multi-body system [24]:

$$\begin{bmatrix} \mathbf{M} & \Psi_{,X}^T \\ \Psi_{,\mathbf{X}} & 0 \end{bmatrix} \begin{bmatrix} \ddot{X} \\ \Lambda \end{bmatrix} = \begin{bmatrix} \mathbf{C} \\ -\dot{\Psi}_{,\mathbf{X}} \dot{X} \end{bmatrix} + \begin{bmatrix} \mathbf{F} \\ 0 \end{bmatrix} \tag{17}$$

where $\mathbf{M}$ is the generalized mass matrix of the multi-body:

$$\mathbf{M} = \begin{bmatrix} \mathbf{E}m_1 & -m_1 {}_{O_1}{}^{I}\tilde{r}_{cm_1} & \cdots & 0 & \\ m_1 {}_{O_1}{}^{I}\tilde{r}_{cm_1} & {}_{O_1}{}^{I}\mathbf{I}_1 & & & \\ \vdots & & \ddots & \vdots & \\ & & & \mathbf{E}m_N & -m_N {}_{O_N}{}^{I}\tilde{r}_{cm_N} \\ 0 & & \cdots & m_N {}_{O_N}{}^{I}\tilde{r}_{cm_N} & {}_{O_N}{}^{I}\mathbf{I}_N \end{bmatrix} \tag{18}$$

and $\mathbf{E}$ is a 3×3 identity matrix. The vector $\mathbf{C}$ contains all terms that do not depend on the second derivatives in Eq. (13) and Eq. (14) and $\mathbf{F}$ is the generalized external force vector acting on the bodies.

2.3. Governing equations of the floating multibody spacecraft with a minimum set unknown

The problems highlighted at the end of the previous section can be avoided by transforming the system of Eq. (17) into a new one where the Lagrangian multipliers disappear. This means that a new set of kinematic Degrees of Freedom (DOF), which automatically satisfies the compatibility equations, must be introduced. From a mechanics point of view it implies the reduction of the kinematics parameters of the system. From a practical point of view it can be done by projecting the translational and rotational DOF of the multibody along the directions of the allowed relative motion, where constraint reactions do not have any components. This can be done by expressing the state vector as a function of the joints velocities as reported in Eq. (10) leading to:

$$\begin{bmatrix} \mathbf{M} & \Psi_{,X}^T \\ \Psi_{,\mathbf{X}} & 0 \end{bmatrix} \begin{bmatrix} \mathbf{J} & 0 \\ 0 & \mathbf{E} \end{bmatrix} \begin{bmatrix} \ddot{Q} \\ \Lambda \end{bmatrix} + \begin{bmatrix} \mathbf{M} & \Psi_{,X}^T \\ \Psi_{,\mathbf{X}} & 0 \end{bmatrix} \begin{bmatrix} \dot{\mathbf{J}} & 0 \\ 0 & 0 \end{bmatrix} \begin{bmatrix} \dot{Q} \\ 0 \end{bmatrix} = \begin{bmatrix} \mathrm{C} \\ -\dot{\Psi}_{,\mathbf{X}} \mathbf{J} \dot{Q} \end{bmatrix} + \begin{bmatrix} \mathrm{F} \\ 0 \end{bmatrix} \tag{19}$$

It can be demonstrated that the Jacobian matrix $\mathbf{J}$, appearing in Eq. (19), is the space-null of the joint constraint matrix $\Psi_{,\mathbf{X}}$ (see Refs. [1,15]) where:

$$\Psi_{,\mathbf{X}} \mathbf{J} = 0 \tag{20}$$

By deriving Eq. (20) with respect to time it is possible to obtain:

$$\dot{\Psi}_{,\mathbf{X}} \mathbf{J} + \Psi_{,\mathbf{X}} \dot{\mathbf{J}} = 0 \tag{21}$$

Pre-multiplying Eq. (19) by $\mathbf{J}^T$ and considering Eq. (20) one can obtain:

$$\mathbf{J}^T \mathbf{M} \mathbf{J} \ddot{Q} = \mathbf{J}^T \mathrm{C} + \mathbf{J}^T \mathrm{F} - \mathbf{J}^T \mathbf{M} \dot{\mathbf{J}} \dot{Q} \tag{22}$$

this represents the minimum set of ODE equations representing the dynamics of the multibody. It is interesting to observe that Eq. (22) is practically equivalent to the system of equations that could be derived by using a classical Lagrangian approach where all the degrees of freedom are chosen kinematically compatible with the constraints [24].

By considering the definition of the reduced space state in Eq. (12), it is possible to rewrite Eq. (22) as:

$$\begin{bmatrix} \mathbf{B}_{\pi\pi} & \mathbf{B}_{\pi\eta} \\ \mathbf{B}_{\eta\pi} & \mathbf{B}_{\eta\eta} \end{bmatrix} \begin{bmatrix} \ddot{Q}_\pi \\ \ddot{Q}_\eta \end{bmatrix} + \begin{bmatrix} \Sigma_\pi \\ \Sigma_\eta \end{bmatrix} = \begin{bmatrix} \mathrm{F}_\pi \\ \mathrm{F}_\eta \end{bmatrix} + \begin{bmatrix} 0 \\ \tau_\eta \end{bmatrix} \tag{23}$$

where Q_π is the vector of six components (3 displacement and 3 rotations) of the first body of the kinematic chain. The vector Q_η represents the joint variables, whereas Σ_π and Σ_η are nonlinear terms. The vectors F_π and F_η are the external generalized forces applied to the first body and along the joint directions, respectively.

2.4. Gravity and gravity gradient forces

The floating condition of the spacecraft is only an approximation of the real environment conditions in which the spacecraft has to operate. In particular the leading perturbing force acting on the satellite is due to the gravitational field whose effects influence the translational and rotational motion of the spacecraft as well. The mathematical expression for the gravitational forces and torques acting on each body are well known [10]:

$${}^{I}\vec{F}_{b_i}^{grav} = -m_i \frac{\mu_\oplus}{{}_{O_I}{}^{I}r_{O_i}^3} {}_{O_I}{}^{I}\vec{r}_{O_i} \tag{24}$$

$${}_{O_i}{}^{I}\vec{M}_{b_i}^{grav} = -m_i \frac{\mu_\oplus}{{}_{O_I}{}^{I}r_{O_i}^3} {}_{O_i}{}^{I}\tilde{r}_{cm_i\,O_I}{}^{I}\vec{r}_{O_i} + \frac{3\mu_\oplus}{{}_{O_I}{}^{I}r_{O_i}^3} {}_{O_I}{}^{I}\tilde{\hat{r}}_{O_i\,O_i}{}^{I}\mathbf{I}_{b_i\,O_I}{}^{I}\hat{r}_{O_i} \tag{25}$$

where $\mu_\oplus$ is the Earth gravitational constant. These forces must be 'assembled' as follows:

$$\mathrm{F}^{grav} = \begin{bmatrix} {}^{I}\vec{F}_{b_1}^{gravT} & {}_{O_1}{}^{I}\vec{M}_{b_1}^{gravT} & {}^{I}\vec{F}_{b_2}^{gravT} & {}_{O_2}{}^{I}\vec{M}_{b_2}^{gravT} \\ \cdots & {}^{I}\vec{F}_{b_N}^{gravT} & {}_{O_N}{}^{I}\vec{M}_{b_N}^{gravT} \end{bmatrix}^T \tag{26}$$

and then projected along the joint allowed directions of the multibody by means of the Jacobian matrix, leading to:

$$\begin{bmatrix} \mathrm{F}_\pi^{grav} \\ \mathrm{F}_\eta^{grav} \end{bmatrix} = \mathbf{J}^T \mathrm{F}^{grav} \tag{27}$$

The terms F_π^{grav} and F_η^{grav} appearing in Eq. (27) are the generalized gravitational forces acting on the hosting base of the manipulator and along its joint directions respectively.

3. Deployment control strategies

In this section three different control strategies to deploy a space manipulator are presented and eventually compared with each other. The idea is to evaluate the advantages and the drawbacks in terms of control efforts to accomplish a complete deploying maneuver. The control strategies here addressed are:

- Proportional derivative control (Eq. (28)).
- Jacobian transpose control (Eq. (29)).
- Reaction null control.

An evaluation of the benefits and the drawbacks of these control strategies are given in the next section, where they are applied to a space based manipulator system. A detailed explanation of the first two control strategies is given in [27] whereas the reaction null control approach here used is based on Refs. [6,7,35].

In particular for the well-known PD control the torque at the i-th joint reads as follows:

$$\tau_{\eta_i} = -k_{p_i}(\vartheta_i - \chi_i) - k_{d_i}(\dot{\vartheta}_i - \dot{\chi}_i) \tag{28}$$

where k_{p_i}, k_{d_i} are the proportional and derivative gains and χ_i, $\dot{\chi}_i$ are the desired joint positions and velocities when the end-effector reaches the target. The JTC control of the joint motors can be computed as follows:

$$\tau_\eta = -\mathbf{J}_{ee}^T \left[\mathbf{K}_p^{ee} \left({}_\pi^\pi\vec{r}_{ee} - {}_\pi^\pi\vec{r}_{ee}^{\,d} \right) + \mathbf{K}_d^{ee} \left({}_\pi^\pi\dot{\vec{r}}_{ee} - {}_\pi^\pi\dot{\vec{r}}_{ee}^{\,d} \right) \right] - \mathbf{K}_d^\eta \dot{Q}_\eta \tag{29}$$

being $\mathbf{J}_{ee}$ the Jacobian matrix of the end effector, ${}_\pi^\pi\vec{r}_{ee}$ and ${}_\pi^\pi\vec{r}_{ee}^{\,d}$ the actual and desired positions of the end effector with respect to the

base platform. Moreover ${}^{\pi}_{\pi}\dot{\vec{r}}_{ee}$, ${}^{\pi}_{\pi}\dot{\vec{r}}^{d}_{ee}$ are their time derivatives, $\mathbf{K}^{ee}_{p}$ and $\mathbf{K}^{ee}_{d}$ are the gain matrices respectively for the end effector position and velocity errors [5]. A brief summary of the reaction null characteristics controls is reported in the following section in order to explain how the reaction null can compensate the gravitational forces.

3.1. Reaction null control

A useful centralized control strategy is the reaction null method, which allows a reduction of the control effort to maintain a correct attitude of the spacecraft. The main goal of this method is to perform a manipulator manoeuver without affecting the base attitude and position. In particular, given a desired and planned joints trajectories $\chi(t)$, or the target end effector positions ${}^{\pi}_{\pi}\vec{r}_{ee}(t)$, this control allows to follow them by imposing a *hard* constraint: no reaction forces and torques must be transmitted to the hosting spacecraft. These tasks can be performed by a constrained optimization problem by taking, as a Hamiltonian cost function, the following expression [6]:

$$H(\dot{Q}_{\eta},\lambda_{\pi}) = \frac{1}{2}(\dot{Q}_{\eta}-\dot{\chi})^{T}(\dot{Q}_{\eta}-\dot{\chi}) + \lambda^{T}_{\pi}(B_{\pi\eta}\dot{Q}_{\eta}) \tag{30}$$

where λ_{π} is the vector containing the Lagrange multipliers used to guarantee the constraint of zero dynamic coupling between the manipulator and the spacecraft (i.e. no variation of the linear and angular momentum of the platform when the robotic arms move). The necessary conditions for solving the proposed constrained optimization problem are [3]:

$$\begin{aligned}\frac{\partial}{\partial\dot{Q}_{\eta}}H(\dot{Q}_{\eta},\lambda_{\pi})^{T} &= 0\\ \frac{\partial}{\partial\lambda_{\pi}}H(\dot{Q}_{\eta},\lambda_{\pi})^{T} &= 0\end{aligned} \tag{31}$$

that brings to the following conditions:

$$\dot{Q}_{\eta} = \mathbf{B}^{T}_{\pi\eta}\lambda_{\pi} + \dot{\chi} \tag{32}$$

$$B_{\pi\eta}\dot{Q}_{\eta} = 0 \tag{33}$$

By substituting Eq. (32) into Eq. (33), and by defining the pseudo-inverse matrix as follows:

$$\mathbf{B}^{*}_{\pi\eta} = \mathbf{B}^{T}_{\pi\eta}\left(\mathbf{B}_{\pi\eta}\mathbf{B}^{T}_{\pi\eta}\right)^{-1} \tag{34}$$

one obtains the optimal solution of the manipulator motion:

$$\dot{Q}_{\eta} = \left[\mathbf{E}-\mathbf{B}^{*}_{\pi\eta}\mathbf{B}_{\pi\eta}\right]\dot{\chi} = \mathbf{N}_{s}\dot{\chi} \tag{35}$$

The matrix $\mathbf{N}_{s}$ is called null-space matrix of $\mathbf{B}_{\pi\eta}$ because it satisfies the following property:

$$\mathbf{B}_{\pi\eta}\mathbf{N}_{s} = 0 \tag{36}$$

Eq. (36) can be used not only to constrain all the DOFs of the base platform, but also it can be re-arranged in order to avoid the disturbance only in a number of pre-selected subspace of the base platform angular velocity variables. In the present study the adopted RNS control will avoid the influence of the motion of the arms on the angular velocity of the platform [6] only.

By deriving and then substituting Eq. (35) and Eq. (36) in the platform's equations of motion (described by the matrices $\mathbf{B}_{\pi\pi}$ and $\mathbf{B}_{\pi\eta}$ in Eq. (23)) it is possible to obtain the required joint control torques:

$$\tau_{\eta} = \mathbf{B}_{\eta\eta}\mathbf{N}_{s}\ddot{\chi} - \mathbf{B}_{\eta\eta}\mathbf{B}^{*}_{\pi\eta}\tilde{\Sigma}_{\pi} + \tilde{\Sigma}_{\eta} \tag{37}$$

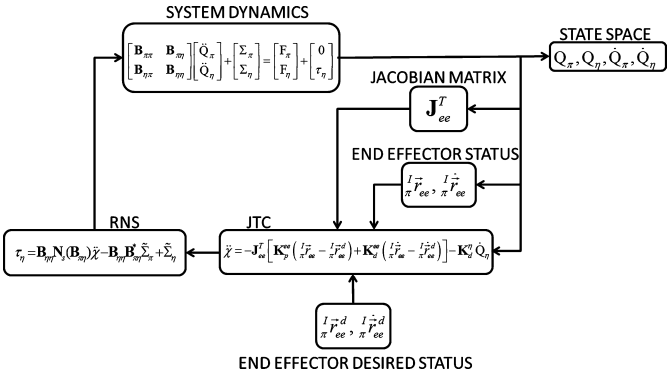

Fig. 3. Control scheme of the RNS–JTC.

where $\tilde{\Sigma}_{\pi}$ and $\tilde{\Sigma}_{\eta}$ are defined as

$$\tilde{\Sigma}_{\pi} = \Sigma_{\pi} - \left[\mathbf{J}^{T}\,\mathrm{F}^{e}\right]_{\pi}, \qquad \tilde{\Sigma}_{\eta} = \Sigma_{\eta} - \left[\mathbf{J}^{T}\,\mathrm{F}^{e}\right]_{\eta} \tag{38}$$

The terms $[\mathbf{J}^{T}\,\mathrm{F}^{e}]_{\pi}$ and $[\mathbf{J}^{T}\,\mathrm{F}^{e}]_{\eta}$ are the projections of the generalized external forces F^{e} acting on the space system on the minimum space of the joints. In the following the generalized vector F^{e} contains the gravity and gravity gradient forces acting on each body of the systems. It is interesting to observe that Eq. (38) also guarantees the compensation of the gravitational forces by the reaction null controller.

These are the required torques that must be provided by the motors in order to respect the zero reaction condition to the hosting spacecraft. In order to use the control law reported in Eq. (37) it is necessary to define the function $\ddot{\chi}$ which represents the desired motion of the joints. For the case under concern this function has been chosen to follow the dynamics provided by the JTC.

$$\ddot{\chi} = -\mathbf{J}^{T}_{ee}\left[\mathbf{K}^{ee}_{p}\left({}^{\pi}_{\pi}\vec{r}_{ee} - {}^{\pi}_{\pi}\vec{r}^{d}_{ee}\right) + \mathbf{K}^{ee}_{d}\left({}^{\pi}_{\pi}\dot{\vec{r}}_{ee} - {}^{\pi}_{\pi}\dot{\vec{r}}^{d}_{ee}\right)\right] - \mathbf{K}^{\eta}_{d}\dot{Q}_{\eta} \tag{39}$$

In Fig. 3 a mixed control strategy, that in the following we refer as Reaction Null Space–Jacobian Transpose Control (RNS–JTC), is reported. It is obtained by substituting Eq. (39) into Eq. (37), as shown in the figure. This control can be interpreted as a filtered version of the simple Jacobian Transpose Control that, through the use of the reaction null controller, eliminates the interaction between the attitude of the base and the motion of its arms.

4. Numerical results

The dynamic equations and the control schemes seen in the previous sections are applied for studying the deploying maneuver of robotic space manipulators. The control strategies described in Section 3 are also compared in terms of efficiency and power control effort when a deploying maneuver is assigned. The spacecraft platform hosting the space manipulator and the geometrical and inertia characteristics of the robotic arms necessary for the simulations are reported in Section 4.1.

4.1. Space manipulator system characteristics

The system chosen for the simulation is schematically reported in Fig. 4. The spacecraft is constituted by a central cubic platform, whose geometrical and inertia properties are shown in Table 1.

Two identical arms are attached to the two opposite sides of the hosting platform. Each of them is constituted by 6 links interconnected by revolute joints, modeled as ideal ones, obtaining a kinematic chain as depicted in Fig. 5, where the joints are represented by red cylinders whose longitudinal axes are the directions

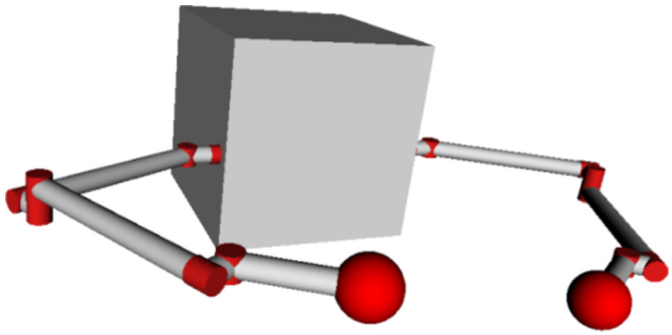

Fig. 4. Layout of the space manipulator.

Table 1
Geometrical and inertia properties of the spacecraft central bus.

Dimensions		Centre of mass position	
L (m)	2.0	G (m)	[0, 0, 0]
Mass		Moments of inertia	
m_s (kg)	500	$I_{xx} = I_{yy} = I_{zz}$ (kg m^2)	333.33

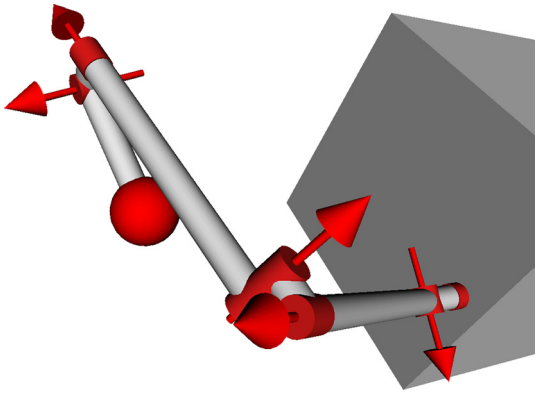

Fig. 5. Layout of the revolute joints and their rotation axis represented by the arrows.

Table 2
Geometrical and inertia properties of the manipulator links.

Dimensions	L1	L2	L3	L4	L5	L6
L_x (m)	0.30	1.60	0.20	1.60	0.20	0.80
R_{int} (m)	0.06	0.06	0.06	0.06	0.06	0.06
R_{est} (m)	0.08	0.08	0.08	0.08	0.08	0.08
Centre of mass position						
G_x (m)	0.00	0.69	0.00	0.00	0.04	0.12
G_y (m)	0.00	0.00	0.00	−0.69	0.00	0.00
G_z (m)	0.08	0.00	0.04	0.00	0.00	0.00
Moments of inertia						
I_{xx} (kg m^2)	0.23	0.19	0.09	32.52	0.02	0.05
I_{yy} (kg m^2)	0.23	32.52	0.08	0.19	0.08	0.53
I_{zz} (kg m^2)	0.05	32.54	0.02	32.54	0.09	0.55
Mass						
m_l (kg)	13.12	44.00	10.75	44.00	10.75	25.00

of revolution of the joints. Their geometrical characteristics and their inertia properties are listed in Table 2. It is worth to note that the geometry, the inertia properties and the dimensions here used must be considered as an example of a space system. The end effector is, for simplicity, geometrically represented as a point mass, attached to the last link of the manipulator.

As previously mentioned the manipulator deploying maneuver phases will be analyzed with a particular focus on the control efforts necessary to perform these tasks. All the analyses will be performed by considering an orbiting spacecraft whose initial conditions are reported in Table 3.

Table 3
Initial conditions of the base platform.

	x axis	y axis	z axis
Linear velocity vector (km/s)	7.47	0.00	0.00
Angular velocity vector (deg/s)	0	0	0
Position vector (km)	0	−7145	0
Euler angles (deg)	0	0	0

For the case of a single arm system, the Jacobian matrix in Eq. (22) has the following expression:

$$\begin{bmatrix} {}^{I}\dot{X}_{bp} \\ {}^{I}_{I}\omega_{bp} \\ {}^{I}\dot{X}_{l1} \\ {}^{I}_{I}\omega_{l1} \\ \vdots \\ {}^{I}\dot{X}_{l6} \\ {}^{I}_{I}\omega_{l6} \end{bmatrix} = \begin{bmatrix} I & 0 & 0 & 0 \\ 0 & I & 0 & 0 \\ I & -{}_{O_{bp}}{}^{I}\tilde{d}_{j1} & 0 & 0 \\ 0 & I & {}^{I}\hat{z}_{j1} & 0 \\ \vdots & \vdots & \vdots & \vdots \\ I & -{}_{O_{bp}}{}^{I}\tilde{d}_{j1} & -{}_{O_{l1}}{}^{I}\tilde{d}_{j2}\,{}^{I}\hat{z}_{j1} & -{}_{O_{l2}}{}^{I}\tilde{d}_{j3}\,{}^{I}\hat{z}_{j2} \\ 0 & I & {}^{I}\hat{z}_{j1} & {}^{I}\hat{z}_{j2} \end{bmatrix}$$

$$\begin{bmatrix} 0 & 0 & 0 & 0 \\ 0 & 0 & 0 & 0 \\ 0 & 0 & 0 & 0 \\ 0 & 0 & 0 & 0 \\ \vdots & \vdots & \vdots & \vdots \\ -{}_{O_{l3}}{}^{I}\tilde{d}_{j4}\,{}^{I}\hat{z}_{j3} & -{}_{O_{l4}}{}^{I}\tilde{d}_{j5}\,{}^{I}\hat{z}_{j4} & -{}_{O_{l5}}{}^{I}\tilde{d}_{j6}\,{}^{I}\hat{z}_{j5} & 0 \\ {}^{I}\hat{z}_{j3} & {}^{I}\hat{z}_{j4} & {}^{I}\hat{z}_{j5} & {}^{I}\hat{z}_{j6} \end{bmatrix} \begin{bmatrix} {}^{I}\dot{X}_{bp} \\ {}^{I}_{I}\omega_{bp} \\ \dot{Q}_{\eta 1} \\ \dot{Q}_{\eta 2} \\ \dot{Q}_{\eta 3} \\ \dot{Q}_{\eta 4} \\ \dot{Q}_{\eta 5} \\ \dot{Q}_{\eta 6} \end{bmatrix} \tag{40}$$

where ${}_{O_{bp}}{}^{I}\tilde{d}_{j1}$ represents the skew-symmetric matrix of the position vector of the joint 1 with respect to the origin of the reference frame of the base platform (O_{bp}), projected in the inertial reference frame (I). The term ${}_{O_{l1}}{}^{I}\tilde{d}_{j2}$ represents the skew-symmetric matrix of the position vector of the joint 2 with respect to the origin of the reference frame of the first link (O_{l1}), projected to the inertial reference frame (I), and similar definitions can be addressed for the matrices ${}_{O_{l2}}{}^{I}\tilde{d}_{j3}$, ${}_{O_{l3}}{}^{I}\tilde{d}_{j4}$, ${}_{O_{l4}}{}^{I}\tilde{d}_{j5}$, ${}_{O_{l5}}{}^{I}\tilde{d}_{j6}$. The unit vectors ${}^{I}\hat{z}_{j1}$, ${}^{I}\hat{z}_{j2}$, ${}^{I}\hat{z}_{j3}$, ${}^{I}\hat{z}_{j4}$, ${}^{I}\hat{z}_{j5}$ and ${}^{I}\hat{z}_{j6}$ represent the joint directions projected to the inertial reference frame (I). Similar mathematical steps can be done for the second arm of the manipulator and eventually assembled with Eq. (40) in order to obtain the Jacobian matrix of the overall space system. For the case under study the Jacobian matrix has dimension $6N_b \times N_{dof}$ where N_b (= 13) is the number of bodies and N_{dof} (= 18) is the number of DOF (6 for the base platform and 12 for the joints).

4.2. Preliminary deploying analysis using the RNS–JTC

It is well known that a reaction null control does not allow a manipulator to grasp every geometrically reachable target of its surrounding space [16,34]. Therefore it is necessary to find the effective RNS–JTC reachable points in advance. For obtaining these points some preliminary target positions belonging to the surface of semi spheres, centered on the center of mass of the base platform, with different radii (2, 2.25, 2.5, 2.75, 3, 3.25, 3.50, 3.75, 4 meters) are selected. Then different deploying maneuvers are performed for each of these pre-selected target points, checking at the end of them which of these points is effectively reached by the end effector. This parametric study is performed by moving only one of the two arms, maintaining the second one locked in the stowed configuration. It is worth to note that the self-collision

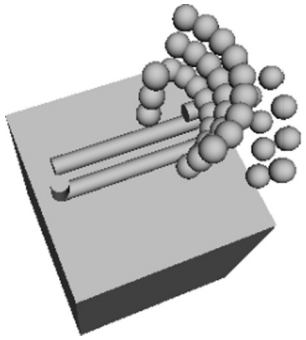

Fig. 6. Sketch of the reaction null reachable points when one arm is fixed (case 1 of Table 5).

avoidance task was not implemented in the control algorithms. Suffice here to say that for the example here proposed no self-collisions were observed during the simulations. The analysis confirms that the RNS–JTC allows to reach a very limited number of possible targets inside the manipulator workspace. In fact for the case under concern only 50 points over the 1500 points analyzed has been effectively reached. Fig. 6 gives a schematic representation of the position of these points around the manipulator. The authors have also observed that these positions do not change when changing the values of the control gains.

To better understand the influence of the control gains on the performance of the controllers a further analysis has been done by evaluating the power required for moving the motors at the joints. To do this an index of power consumption is introduced:

$$C_f = \int_0^{T_f} \sqrt{\sum_{i=1}^{n_{\text{joint}}} \tau_i^2}\, dt + \int_0^{T_f} \sqrt{\tau_\pi^2}\, dt \tag{41}$$

where τ_i is the i-th joint torque, τ_π is the torque applied to the spacecraft platform and T_f is the duration time of the deploying maneuver.

Among all the 50 reachable points, previously found, the one located at $x = 0.2$ m, $y = 0$ m, $z = 3$ m from the center of mass of the base platform has been considered as a reference target point for the power consumption analysis. The analysis has been performed by using as reference control gains the values of $K_p^{ee} = 45$ N and $K_d^{ee} = 55$ N s. These reference gains have been properly chosen in order to complete the maneuver in $T_f = 700$ s. Moreover a variation of the proportional gain is considered by scaling the reference value with a coefficient G_c that varies from 0.1 to 100. In Fig. 7 the time histories of the relative distance Δ_{EE} of the end effector from the target are reported for different values of G_c. It is interesting to observe that when $G_c \geq 1$ the end effector reaches the target position always at the same time instant approximately equal to 700 s. Moreover the authors have observed that the time histories of Δ_{EE}, after a fixed time of about 150 s, are not dependent on the value of the control gains. This behavior is essentially due to the constraint imposed by the RNS–JTC on the motion of the base platform, which allows only one particular trajectory of the joints in order to reach the target, without affecting the spacecraft attitude. Of course the choice of the gains changes the power consumption as shown in Table 4 where the power index consumption C_f is reported. It is interesting to observe that C_f varies almost linearly with G_c. This result was not easily deducible at the beginning of the analyses since the index C_f is proportional to the integral over the time of a combination of control gains multiplied by the angular errors (and of course by the angular rate errors); so an increase in the gains also produces a more rapid maneuver that in turns should reduce its duration. Indeed this is not true when RNS–JTC is applied as shown in Fig. 7,

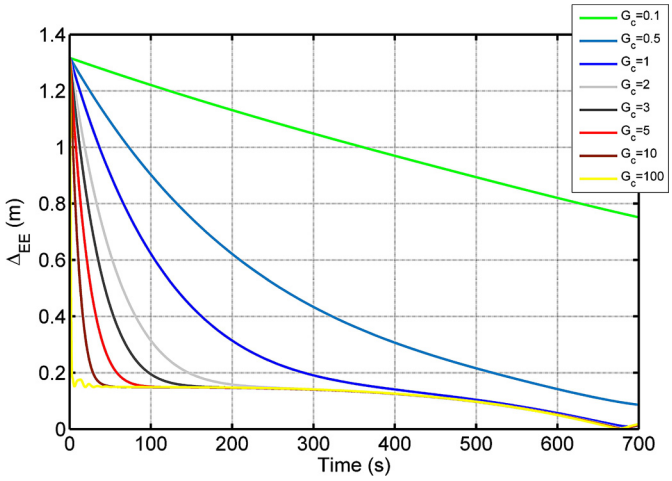

Fig. 7. Time histories of the end effector distance from the target for different values of G_c.

Table 4
Manoeuver consumption index C_f for different values of G_c (RNS–JTC).

G_c	1	2	3	5	10	100
C_f (Nm s)	2.18e−1	4.37e−1	6.55e−1	1.09	2.18	21.4

Table 5
PD control gains for each joint of the manipulator.

Joint	K_p^{pd} (Nm/rad)	K_d^{pd} (Nm s/rad)
1	1.50e−2	7.00e−1
2	4.50e−2	10.00
3	1.80e−3	8.00e−1
4	4.50e−3	1.00
5	1.50e−3	6.00e−1
6	7.50e−4	1.90e−1

where for $G_c \geq 1$ it is clearly visible that the time history of the end effector approaching the target is not affected by the values of the gains used for the control as said above.

4.3. Single manipulator deploying maneuver: controller comparative analyses

The described control strategies have been analyzed in order to compare their effectiveness in terms of power consumption. The control laws studied are the RNS–JTC, the JTC and the PD control. The gains used for the PD controller are reported in Table 5: they are chosen in order to guarantee a duration time of the maneuver of about 700 s. Remember that, for the case under analysis, the duration of the maneuver is not affected by the control gains when the RNS–JTC are employed. The results in terms of the manoeuvre consumption index C_f are summarized in Table 6. It is interesting to observe that the RNS–JTC produces a higher power consumption with respect to the JTC and the PD controllers at the end of the manoeuvre. To better understand these results, a deeper investigation of the RNS–JTC is performed in Section 4.5.

Finally in Fig. 8, Fig. 9 and Fig. 10 screenshots, representing the deployment configurations of the robotic arm, are reported. It is interesting to observe that in the case of the RNS–JTC and of the JTC the end effector arrives nearby the target in approximately 300 s. The remaining 400 s are used by the controller for reaching and eventually grasping the target. A slightly different behavior is obtained by using the PD controller. In fact in this case, after 300 s, the end effector is still far from the target although the grasping mission is accomplished in 700 s as the previous ones.

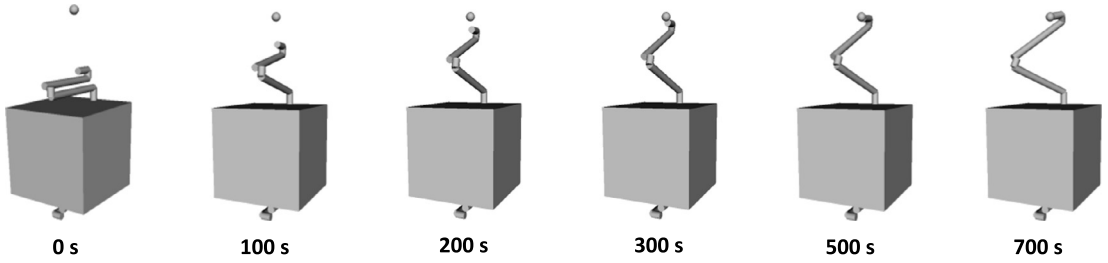

Fig. 8. Time sequence of the RN–JTC maneuver.

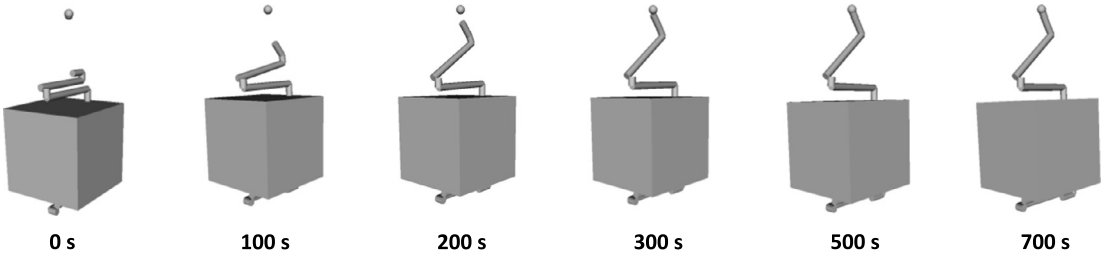

Fig. 9. Time sequence of the JTC maneuver.

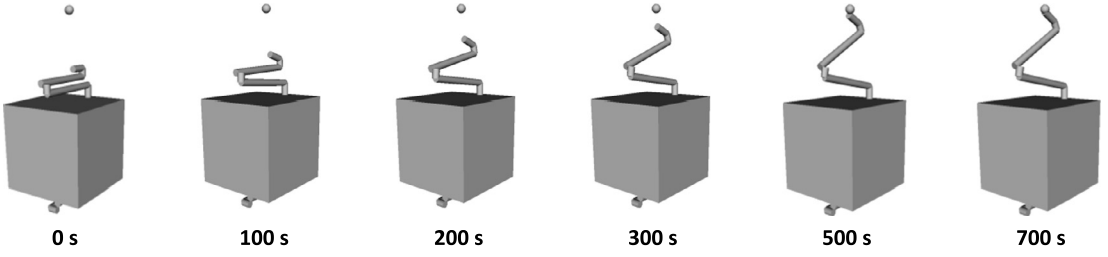

Fig. 10. Time sequence of the PD control maneuver.

Table 6
Maneuver consumption for RNS–JTC and JTC control strategies.

Joint	RNS–JTC C_f (Nms)	JTC C_f (Nms)	PD C_f (Nms)
1	6.45e−4	6.43e−4	1.40e−4
2	1.05e−2	1.10e−3	4.56e−4
3	1.90e−2	6.46e−4	1.71e−4
4	1.44e−2	1.60e−3	4.70e−4
5	1.25e−4	2.66e−4	5.36e−5
6	4.22e−4	1.69e−4	1.07e−4
Base platform	0.00	3.50e−3	1.37e−3
Total cons.	1.80e−2	5.70e−3	4.42e−3

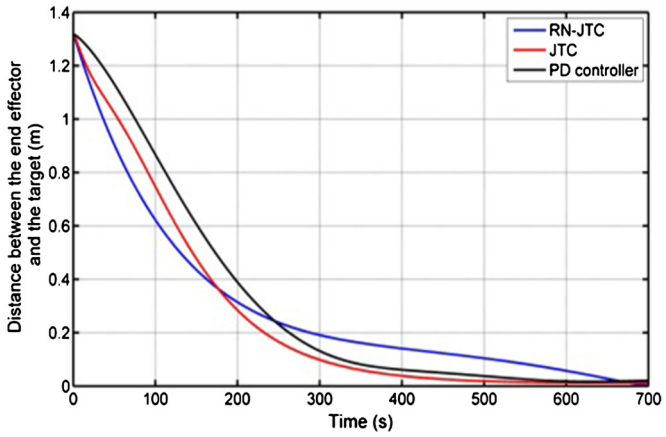

Fig. 11. Time histories of the distance between the end effector and the target.

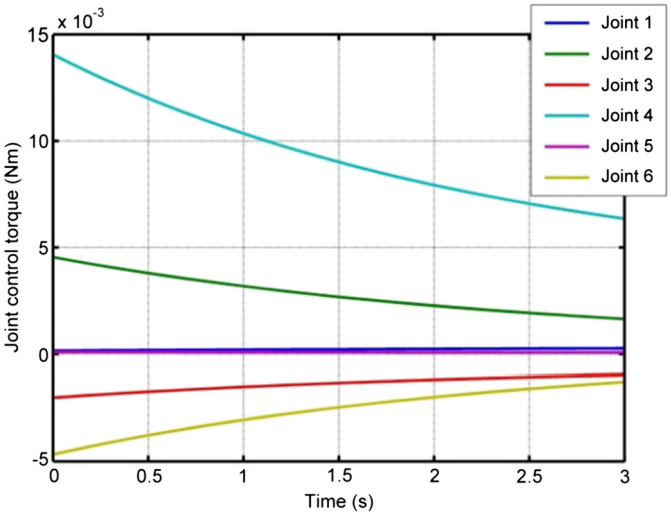

Fig. 12. Joint control torques time histories with JTC.

Fig. 11 shows the distance between the end-effector and the target for the above control strategies.

The control effort differences between the RNS–JTC and JTC appear mainly in the first phase of the deploying maneuver, as it can be observed in Fig. 12 and Fig. 13, where the time histories of the control torques during the first 3 seconds are reported. This difference can be explained by the fact that the resulting torques are higher for the RNS–JTC than the ones required by the simple JTC to perform the same task. Of course this affects the power con-

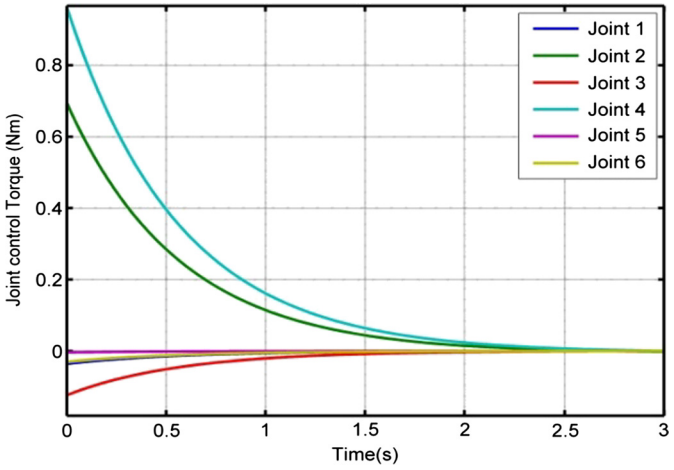

Fig. 13. Joint control torques time histories with RNS–JTC.

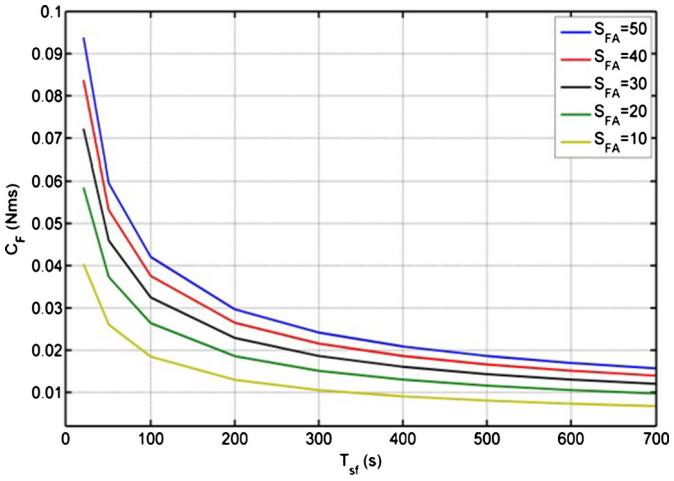

Fig. 14. Consumption trend of the RNS–JTC control.

sumption. To investigate this behavior a further analysis has been performed and the relevant results are reported in the following paragraph.

4.4. Gain improvement for the RNS–JTC

In order to reduce the control effort required by the RNS–JTC during the first part of the deploying a scale factor $S_f(t)$ is introduced to the control scheme, as shown in Eq. (42) and Eq. (43):

$$\tau_{\text{RN–JTC}} = \tilde{\mathbf{B}}_{\eta\eta}\mathbf{N}_s(\tilde{\mathbf{B}}_{\pi\eta})\ddot{\chi} - \tilde{\mathbf{B}}_{\eta\eta}\tilde{\mathbf{B}}^{*}_{\pi\eta}(\tilde{\Sigma}_{\pi}) + \tilde{\Sigma}_{\eta} \tag{42}$$

where:

$$\ddot{\chi} = -S_f\mathbf{J}^{T}_{ee}\left[G_c\mathbf{K}^{ee}_{p}\left({}^{\pi}_{\pi}\vec{r}_{ee} - {}^{\pi}_{\pi}\vec{r}^{d}_{ee}\right) + \mathbf{K}^{ee}_{d}\left({}^{\pi}_{\pi}\dot{\vec{r}}_{ee} - {}^{\pi}_{\pi}\dot{\vec{r}}^{d}_{ee}\right)\right] - S_f\mathbf{K}^{\eta}_{d}\dot{Q}_{\eta} \tag{43}$$

The scale factor $S_f(t)$ is here used to smooth the control action during the first phase of the deploying. A sinusoidal shape function is chosen until a fixed time t_{sf} is reached, then the value of $S_f(t)$ is maintained constant:

$$\begin{cases} S_f = S_{fA}\sin\left(\dfrac{\pi}{2t_{sf}}t\right) & t \le t_{sf} \\ S_f = S_{fA} & t > t_{sf} \end{cases} \tag{44}$$

Of course the choice of the parameters S_{fA} and t_{sf} can be done in several ways. In this case a parametric variation of S_{fA} and

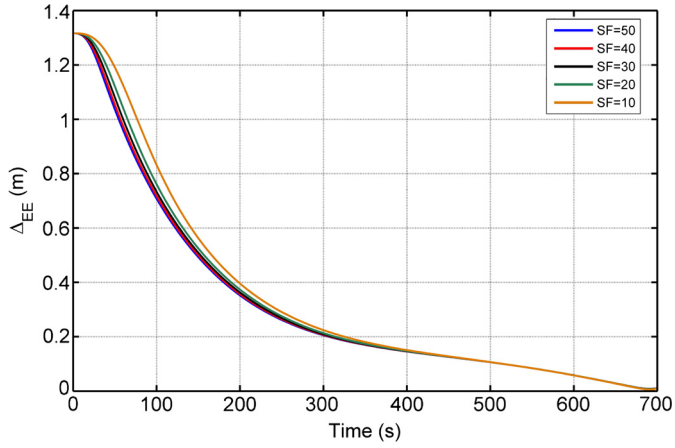

Fig. 15. Time histories of the distance between the end effector and the target by varying S_{fA} and $t_{sf} = 700$ s.

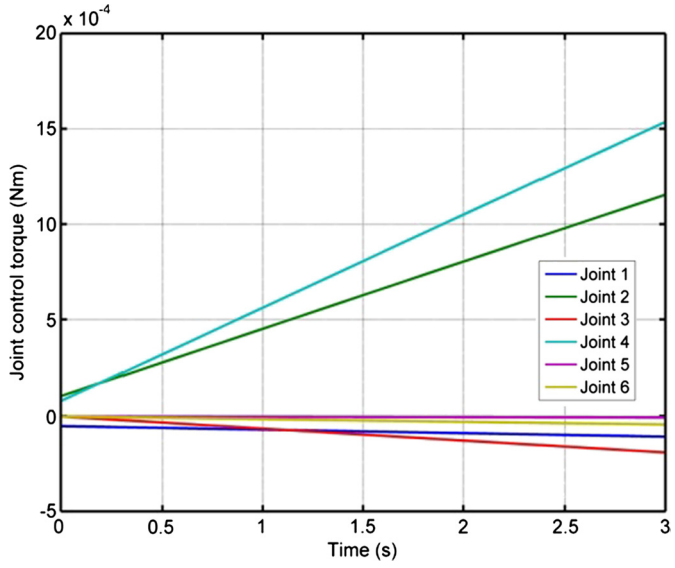

Fig. 16. RNS–JTC Control time history, $S_{fA} = 10$ and $t_{sf} = 700$ s.

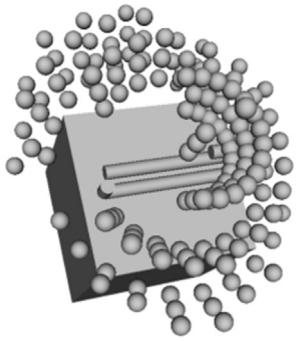

Fig. 17. Sketch of the reaction null reachable points when both arms move.

t_{sf} has been chosen in order to compare the control effort C_f. In Fig. 14 the time histories of the control effort index C_f for different values of the parameter S_{fA} are reported. It is clearly evident that the minimum power consumption corresponds to the values of $S_{fA} = 10$ and $t_{sf} = 700$ s, leading to a value of $C_f = 4.45\text{e}{-3}$ Nms which is of the same order of magnitude as the one obtained for the PD and the JTC controllers analyzed in the previous section.

In Fig. 15 the time histories of distances between the end effector and the target for values of S_{fA} are shown. Values of about

Fig. 18. Screenshots of the symmetric approaching maneuver to the target using the RNS–JTC.

Fig. 19. Screenshot of the non-symmetric approaching maneuver to the target using the RN–JTC.

$S_{fA} < 10$ are not reported here since the authors observe that in these cases they do not guarantee the reachability of the target. Finally in Fig. 16 the control torques obtained by choosing the parameters ($S_{fA} = 10$ and $t_{sf} = 700$ s) are reported for the first 3 seconds of the maneuver. It is very important to note that these torques are now less than the ones reported in Fig. 13 on account of the smoothing applied to the RNS–JTC via the function $S_f(t)$. Note also that they are not null at $t = 0$ even if the gains are null at the beginning. This can be easily explained by the presence of the second and third terms appearing in the right side of Eq. (42) that are not directly dependent on the gains.

4.5. Maneuvers with a double robotic arm

A further analysis has been done by using both the arms of the spacecraft. In particular the second manipulator can be used for: a) the increasing of the workspace of the first arm or b) the grasping of a second target. The task of case a) is proved by performing a similar parametric analyses reported in Section 4.2 by unlocking the joints of the second arm which are now free to move under the Reaction Null Control to compensate the angular velocity of the base. This, in turn, increases the points reached by the end effector of the first manipulator considerably up to about 200 points as shown in Fig. 17.

As far as the task of case b) is concerned we assumed that the second arm must grasp a second target point. The targets for both arms are chosen in order to perform symmetric and non-symmetric maneuvers. In the symmetric case the target grasping points are located at $x = 3.5$ m, $y = -0.1$ m, $z = 2$ m and $x = 3.5$ m, $y = -0.1$ m, $z = -2$ m from the center of mass of the base platform whereas for the non-symmetric case the target grasping points are located at $x = 3$ m, $y = 0.7$ m, $z = 1.3$ m and $x = 3.5$ m, $y = -0.1$ m, $z = -2$ m. In Fig. 18 a sketch of the configurations assumed by the spacecraft in the symmetric maneuver deployment is shown. The result relevant to the non-symmetrically grasping points is shown in Fig. 19, where the deploying sequence is sketched. Also in this case both arms reach the grasping points in about 700 s, showing that the RNS–JTC can be suitable for a non-symmetric grasping maneuver.

5. Conclusion

In this paper an algorithm for simulating the dynamics of space manipulators has been presented via a multibody formulation. In particular a modified Kane-like method, which allows the reduction of the system equation of motion to a minimum set of equations with a minimum number of variables, has been here detailed including gravity and gravity gradient forces. Furthermore a combination of the well-known Jacobian Transpose control and Reaction Null Control has been proposed and applied in a fully tridimensional multibody problem. Two different cases involving space manipulators are presented. Both the manipulators have been mounted on an orbiting platform in order to analyze different control strategies for the deploying maneuver. In particular their efficiency in terms of the power consumption and of the relevant control efforts have been investigated by comparing the PD, the JTC and the RNS–JTC controls.

The numerical results show, if properly tuned, that the RNS–JTC has the same power consumption as the JTC. On the contrary if their relevant gains are not opportunely chosen, they could bring to a higher power consumption of the motor joints than the one required by the JTC. Furthermore the use of RNS–JTC does not require to employ any kind of attitude control of the base platform. This, of course, could represent a valid option during the final deploying phase of a space manipulator to grasp a nearby target. In fact a possible unwanted disturb during the deployment of the arms if not "automatically" compensated could require the action of the controller of the base. This mutual interaction could lead to an increase of the duration of the overall maneuver that in turn could jeopardize the grasping mission due to the fact that the target, which is moving in a different orbit, could leave the workspace of the orbiting chaser. Finally the proposed RNS–JTC algorithm, implemented with the gravitational force compensation, has shown to guarantee that the deploying maneuver is not sensitive to the choice of the gains of the controllers.

Conflict of interest statement

We wish to confirm that there are no known conflicts of interest associated with this publication and there has been no significant financial support for this work that could have influenced its outcome.

Appendix A. Supplementary material

Supplementary material related to this article can be found online at http://dx.doi.org/10.1016/j.ast.2014.07.012.

References

[1] V.I. Arnold, Mathematical Methods of Classical Mechanics, second edition, Springer, 1989.
[2] R. Boumans, C. Heemskerk, The European robotic arm for the International Space Station, Robot. Auton. Syst. 23 (1) (March 1998) 17–27.
[3] A.E. Bryson, Y.C. Ho, Applied Optimal Control: Optimization, Estimation and Control, Taylor & Francis Pub., 1975.
[4] M. Castronuovo, Active space debris removal: a preliminary mission analysis and design, Acta Astronaut. 69 (2011) 848–859.
[5] J.J. Craig, Introduction to Robotics: Mechanics and Control, 3rd ed., Prentice Hall, 2004.
[6] D.N. Dimitrov, Dynamics and control of space manipulators during a satellite capturing operation, Ph.D Thesis in Aerospace Engineering, Tohoku University, Japan, Feb. 2005.
[7] D.N. Dimitrov, K. Yoshida, Momentum distribution in a space manipulator for facilitating the post-impact control, in: Proceedings of the IEEE/RSJ International Conference on Intelligent Robots and Systems, vol. 4, IROS 2004, 28 Sept.–2 Oct. 2004, 2004, pp. 3345–3350.

[8] P. Gasbarri, A two-dimensional approach to multibody free dynamics in space environment, Acta Astronaut. 51 (12) (Dec. 2002) 831–842.
[9] P. Gasbarri, P. Santini, General background and approach to multibody dynamics for space applications, Acta Astronaut. 64 (11–12) (June 2009) 1224–1251.
[10] P.C. Hughes, Spacecraft Attitude Dynamics, Dover, 2004.
[11] R.N. Jazar, Advanced Dynamics: Rigid Body, Multibody, and Aerospace Applications, Wiley, 2011.
[12] T.R. Kane, Dynamics of nonholomic systems, J. Appl. Mech. 28 (1961) 575–578.
[13] T.R. Kane, D.A. Levinson, Dynamics: Theory and Applications, McGraw Hill book company, 1985.
[14] R. Kumar, R. Hayes, System requirements and design features of Space Station Remote Manipulator System mechanisms, in: The 25th Aerospace Mechanism Symposium, May 1, 1991, JPL, 1991, pp. 15–30.
[15] L. Meirovitch, Methods of Analytical Dynamics, Dover Pub., 2004.
[16] D.N. Nenchev, K. Yoshida, Impact analysis and post-impact motion control issues of a free-floating space robot subject to a force impulse, IEEE Trans. Robot. Autom. 15 (3) (June 1999) S48–557.
[17] S.I. Nishida, S. Kawamoto, Strategy for capturing of a tumbling space debris, Acta Astronaut. 68 (2011) 113–120.
[18] S.I. Nishida, S. Kawamoto, Y. Okawa, F. Terui, S. Kitamura, Space debris removal system using a small satellite, Acta Astronaut. 65 (2009) 95–102.
[19] G.B. Palmerini, M. Sabatini, P. Gasbarri, R. Monti, L. Felicetti, Design of debris removal missions performed by robotic graspers, in: Proceedings of the International Astronautical Congress, Naples, Italy, 2012, IAC-12-C2.2.11, 2012.
[20] L. Patten, et al., International Space Station robotics: a comparative study of ERA, JEMRMS and MSS, in: Proceedings of ASTRA 2002, ESTEC, Noordwijk, The Netherlands, Nov. 19–21, 2002.
[21] P. Rank, et al., The DEOS automation and robotic payload, in: Proceedings of ASTRA, 2011.
[22] M. Sabatini, C. Toglia, P. Gasbarri, G.B. Palmerini, Analysis of guidance control laws for orbiting multibody space manipulators, in: Proceedings of the 59th International Astronautical Congress 2008, vol. 7, IAC 2008, International Astronautical Federation, Curran Associates, Inc., 2008, pp. 4495–4508.
[23] P. Santini, Stability of flexible spacecraft, Acta Astronaut. 3 (9–10) (Sept.–Oct. 1976) 685–713.
[24] P. Santini, P. Gasbarri, Dynamics of multibody systems in space environment: Lagrangian vs. Eulerian approach, Acta Astronaut. 54 (1) (Jan. 2004) 1–24.
[25] A.A. Shabana, Dynamics of Multibody Systems, 3rd ed., Cambridge University Press, 2005.
[26] S.V. Shah, A. Gattupalli, A.K. Misra, Energy optimum reactionless path planning for capture of tumbling orbiting objects using a dual-arm robot, in: Proc. 1st International and 16th National Conference on Machines and Mechanisms, iNaCoMM2013, IIT Roorkee, India, Dec. 18–20, 2013.
[27] B. Siciliano, L. Schiavicco, L. Villani, G. Oriolo, Robotics: Modelling, Planning and Control, Springer, 2009.
[28] SpaceX COTS2 Mission Press Kit, SpaceX/NASA Launch and Mission to Space Station, http://www.nasa.gov/pdf/649910main_cots2_presskit_051412.pdf.
[29] C. Toglia, M. Sabatini, P. Gasbarri, G.B. Palmerini, Flexibility effects in controlled behavior of space manipulators, in: Proceedings of the 59th International Astronautical Congress, vol. 8, IAC 2008, International Astronautical Federation, Curran Associates, Inc., 2008, pp. 5371–5384.
[30] C. Toglia, M. Sabatini, P. Gasbarri, G.B. Palmerini, Optimal target grasping of a flexible space manipulator for a class of objectives, Acta Astronaut. 68 (7–9) (April 2011) 1031–1041.
[31] W. Xu, B. Liang, Y. Xu, Survey of modeling, planning, and ground verification of space robotic systems, Acta Astronaut. 68 (11–12) (2011) 1629–1649.
[32] W. Xu, Y. Liu, B. Liang, X. Wang, Y. Xu, Unified multi-domain modeling and simulation of space robot for capturing a moving target, Multibody Syst. Dyn. 23 (3) (2010) 293–331.
[33] W. Xu, D. Meng, Y. Chen, H. Qian, Y. Xu, Dynamics modeling and analysis of a flexible-base space robot for capturing large flexible spacecraft, Multibody Syst. Dyn. (23 August, 2013), http://dx.doi.org/10.1007/s11044-013-9389-0.
[34] K. Yoshida, D.N. Nenchev, Space robot impact analysis and Satellite-base impulse minimization using reaction null space, in: Proceedings of 1995 IEEE International Conference on Robotics and Automation, Nagoya, Japan, 1995, pp. 1271–1277.
[35] K. Yoshida, D. Nenchev, Space robot impact analysis and satellite base impulse minimization using reaction null space, in: Proc. 1995 IEEE Int. Conf. Robot. Automat., Nagoya, Aichi, Japan, May 1995, 1995, pp. 1271–1277.